Journal of Hazardous Materials 185 (2011) 227–235

Contents lists available at ScienceDirect

Journal of Hazardous Materials

journal homepage: www.elsevier.com/locate/jhazmat

Mechanistic pathways differences between P25-TiO_2 and Pt-TiO_2 mediated CV photodegradation

Huan-Jung Fan [a], Chung-Shin Lu [b], Wen-Lian William Lee [c], Mei-Rung Chiou [a], Chiing-Chang Chen [d,*]

[a] Department of Environmental Engineering, Hung Kung University, Taichung Shien 433, Taiwan, ROC
[b] Department of General Education, National Taichung Nursing College, Taichung 403, Taiwan, ROC
[c] Department of Occupational Safety and Health, Chung-Shan Medical University, Taichung 402, Taiwan, ROC
[d] Department of Science Application and Dissemination, National Taichung University of Education, Taichung 403, Taiwan, ROC

ARTICLE INFO

Article history:
Received 13 May 2010
Received in revised form 5 September 2010
Accepted 6 September 2010
Available online 17 September 2010

Key words:
TiO_2
Crystal Violet
Pt
Dye
HPLC–ESI-MS

ABSTRACT

The Crystal Violet (CV) dye represented one of the major triphenylmethane dyes used in textile-processing and some other industrial processes. Various metals doped titanium dioxide (TiO_2) photocatalysts have been studied intensively for the photodegradation of dye in wastewater treatment. In order to understand the mechanistic detail of the metal dosage on the activities enhancement of the TiO_2 based photocatalyst, this study investigated the CV photodegradation reactions under UV light irradiation using a Pt modified TiO_2 photocatalyst. The results showed that Pt-TiO_2 with 5.8% (W/W) Pt dosage yielded optimum photocatalytic activity. Also the effect of pH value on the CV degradation was well assessed for their product distributions. The degradation products and intermediates were separated and characterized by HPLC–ESI-MS and GC–MS techniques. The results indicated that both the *N*-de-methylation reaction and the oxidative cleavage reaction of conjugated chromophore structure occurred, but with significantly different intermediates distribution implying that Pt doped TiO_2 facilitate different degradation pathways compared to the P25-TiO_2 system.

1. Introduction

From an ecological and physiological point of view, the elimination of toxic chemicals from wastewater is currently one of the most crucial subjects in pollution control. The large amount of dyes used in the dyeing stage of textile manufacturing processes represents an increasing environmental danger due to their refractory carcinogenic nature. Particularly, triphenylmethane dyes were consumed heavily in paper, leather, cosmetic and food industries for the coloring of oil, fats, waxes, varnish, and plastics [1–3]. The photocytotoxicity of triphenylmethane dyes, based on the production of the reactive oxygen species, is intensively studied with regard to the photodynamic treatment [4,5]. However, there is a great concern about the thyroid peroxidase-catalyzed oxidation of the triphenylmethane dyes because the reactions might form various *N*-de-alkylated aromatic amines, whose structures are similar to aromatic amine carcinogens [6].

TiO_2 is broadly used as a photocatalyst for degrading a wide range of organic pollutants because of its nontoxicity, photochemical stability, and low cost [7–9]. Moreover, modified TiO_2 has been intensively studied to increase the photoactivity of TiO_2 by adding noble metals such as Au, Pt, and Ag [10,11]. The proposed mechanism included facilitating electron–hole separation and promoting interfacial electron transfer [12,13]. For example, the role of platinum doped on TiO_2, acting as an electron trap which enhanced the quantum efficiency significantly, and thus favored the oxidation of dye substrates [14–16]. Also, the doped Pt reduced the band gap of TiO_2 which benefits the electron transfers from the valence band to conductive band and increases the quantum efficiency of photocatalyst in visible light region [17–19]. Other work also showed that the metal modified TiO_2 may increase the number of electron trap on catalyst surface and attract more cationic dye [20].

In photocatalytic degradation of *N*-alkyl-containing dyes, two major reaction pathways, namely *N*-dealkylation and the conjugated chromophore cleavage, have been well demonstrated. The preferred pathway is strongly dependent on surface properties of catalyst [21–24]. However, there is no conclusive evidence to support the mechanistic relationship between the adsorption mode and degradation pathway. Thus, Pt-TiO_2 was chosen to argue the interesting mechanistic details of CV dye photodegradation and comparing the differences with pure TiO_2.

* Corresponding author at: Department of Science Application and Dissemination, National Taichung University of Education, No. 140, Min-Shen Road, Taichung 403, Taiwan. Tel.: +886 4 2218 3839; fax: +886 4 2218 3530.
E-mail addresses: ccchen@mail.ntcu.edu.tw, ccchen@ms3.ntcu.edu.tw (C.-C. Chen).

0304-3894/$ – see front matter.
doi:10.1016/j.jhazmat.2010.09.022

2. Experimental

2.1. Materials and preparation of photocatalysts—Pt-TiO_2

H_2PtCl_6 (Aldrich) and CV dye (TCI) were obtained and used without any further purification. Reagent-grade ammonium acetate, sodium hydroxide, nitric acid and HPLC-grade methanol were purchased from Merck. De-ionized water used for this study was purified with a Milli-Q water ion-exchange system (Millipore Co.) for a resistivity of $1.8 \times 10^7\ \Omega$ cm. The P25 TiO_2 nanoparticles were supplied by Degussa. A modification of the photo-deposition method [25] was applied for the synthesis of the Pt loaded TiO_2 photocatalytic materials. An aqueous dispersion of TiO_2 (0.5 g/L) was irradiated with a 125 W mercury lamp for 2 h in the presence of 32 g methanol. Then, 0.1 mM H_2PtCl_6 loaded with 0.05, 0.1, 0.2, 0.5, 1.0, 2.0, and 5.0 mL were added to the solution, respectively. The samples are listed in Table 1. Pt content in the prepared catalysts was checked with both energy dispersive spectroscopy (EDS) and high resolution X-ray photoelectron spectrometer (HR-XPS). At the liquid nitrogen temperature, the BET specific surface areas of the samples were measured with an automatic system (Micromeritics Gemini 2370C) with nitrogen gas as the adsorbate.

2.2. Instruments

Waters ZQ LC/MS system, equipped with a binary pump, a photodiode array detector, an autosampler, and a micromass detector, was used for separation and identification. X-ray powder diffraction (XRD) patterns were recorded on a MAC Science, MXP18 X-ray diffractometer with Cu Kα radiation, operated at 40 kV and 80 mA. Field emission scanning electron microscopy (FE-SEM) measurement was carried out with a field-emission microscope (JEOL JSM-7401F) at an acceleration voltage of 15 kV. An HRXPS measurement was carried out with ULVAC-PHI XPS. The Al Kα radiation was generated with a voltage of 15 kV.

2.3. Procedure and analysis

Aqueous suspensions of CV (100 mL, 50 ppm) and the amounts of catalyst powders were placed in the Pyrex flask. The pH value of the suspensions was adjusted by adding either NaOH or HNO_3 solutions. Prior to irradiation, the suspensions were magnetically stirred in the dark for ca. 30 min to establish adsorption/desorption equilibrium between the dye, and the surface of the catalyst under ambient air-equilibrated conditions. Irradiations were carried out using two UV-365 nm lamps (15 W). At given irradiation time intervals, 5 mL aliquots were collected, centrifuged, and then filtered through a Millipore filter to remove the catalyst particulates. The filtrates were analyzed by HPLC–ESI-MS after the readjustment of the chromatographic conditions in order to make the mobile phase compatible with the working conditions of the mass spectrometer.

3. Results and discussion

3.1. Characterization of the platinized-photocatalysts

There were seven different dosage ratios of Pt-TiO_2, (from 0.7 to 7.1 wt% as shown in Table 1), being prepared, namely Pt-TiO_2-A to G, respectively. The surface morphologies of the Pt-TiO_2 powders were examined with a FE-SEM, and the results demonstrated a highly uniform dispersion of platinum particles on TiO_2 surface in Supplementary material, Fig. 1S. In addition, the BET specific surface area of the TiO_2-powder material showed 55.42 m^2/g for Degussa P25, thus, the platinized catalyst samples did not result in significant changes of specific surface area and pore volume

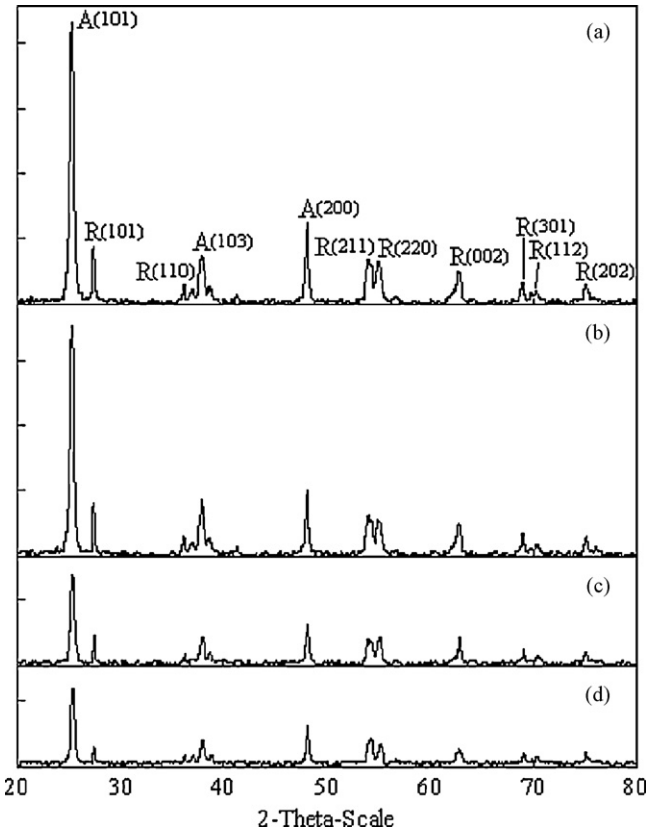

Fig. 1. XRD patterns of the platinum deposits TiO_2 ratios (wt%). (a) P25-TiO_2, (b) Pt-TiO_2-A, (c) Pt-TiO_2-D and (d) Pt-TiO_2-G (A: anatase; R: rutile).

(Table 1). However, there was no characteristic diffraction peak for the Pt0 dopant detected by XRD (Fig. 1). Moreover, the XPS spectrum did show both peaks of 70.0–71.9 eV (Pt $4f_{7/2}$), respectively, representing the TiO_2 modified with platinum (Fig. 2). The results indicated that the photodeposited platinum on the TiO_2 surface could lead Pt(II) being formed, with –O-Pt-O– bonding, then eventually with more Pt(0) grown further on the surface. Both Pt (0) and Pt (II), two chemical states would survive on the TiO_2 surface. A typical two shoulders-peak represented, as the existence for specimen Pt-TiO_2-D, Pt-TiO_2-E, and Pt-TiO_2-F (Fig. 2) demonstrated, the superposition of two-banded spectra for $Pt(OH)_2$ and Pt onto TiO_2 surface [26].

3.2. Effect of Pt-TiO_2 mediated CV photodegradation

The effect of Pt doped on TiO_2 mediated CV photodegradation has been determined. The reaction rates of CV dye photodegradation on seven different dosage ratios of Pt-TiO_2 have been prepared to compare with those on P25-TiO_2 under identical condition (Fig. 3). Interestingly, the presence of Pt content deposits from XPS spectrum have led to a best CV degradation rate, only on an optimal situation of Pt loading up to 5.8 wt% TiO_2 (Pt-TiO_2-F) either under pH 3 or 9. From the curve value shown in Fig. 3a and b, a characteristic agreement shows that photocatalytic activity enhancement depends on Pt content; however, the degradation rate increases first and then decreases with the Pt loading [20,27].

The results have demonstrated that platinum doped TiO_2 enhances the charge separation in semiconductor, and thus increases the energy gap to decrease electron–hole pair recombination (Fig. 4). Noble metal nanoparticle such as platinum is one of the most effective electrons traps, due to the formation of a Schottky barrier at the metal-semiconductor contact. However, for example,

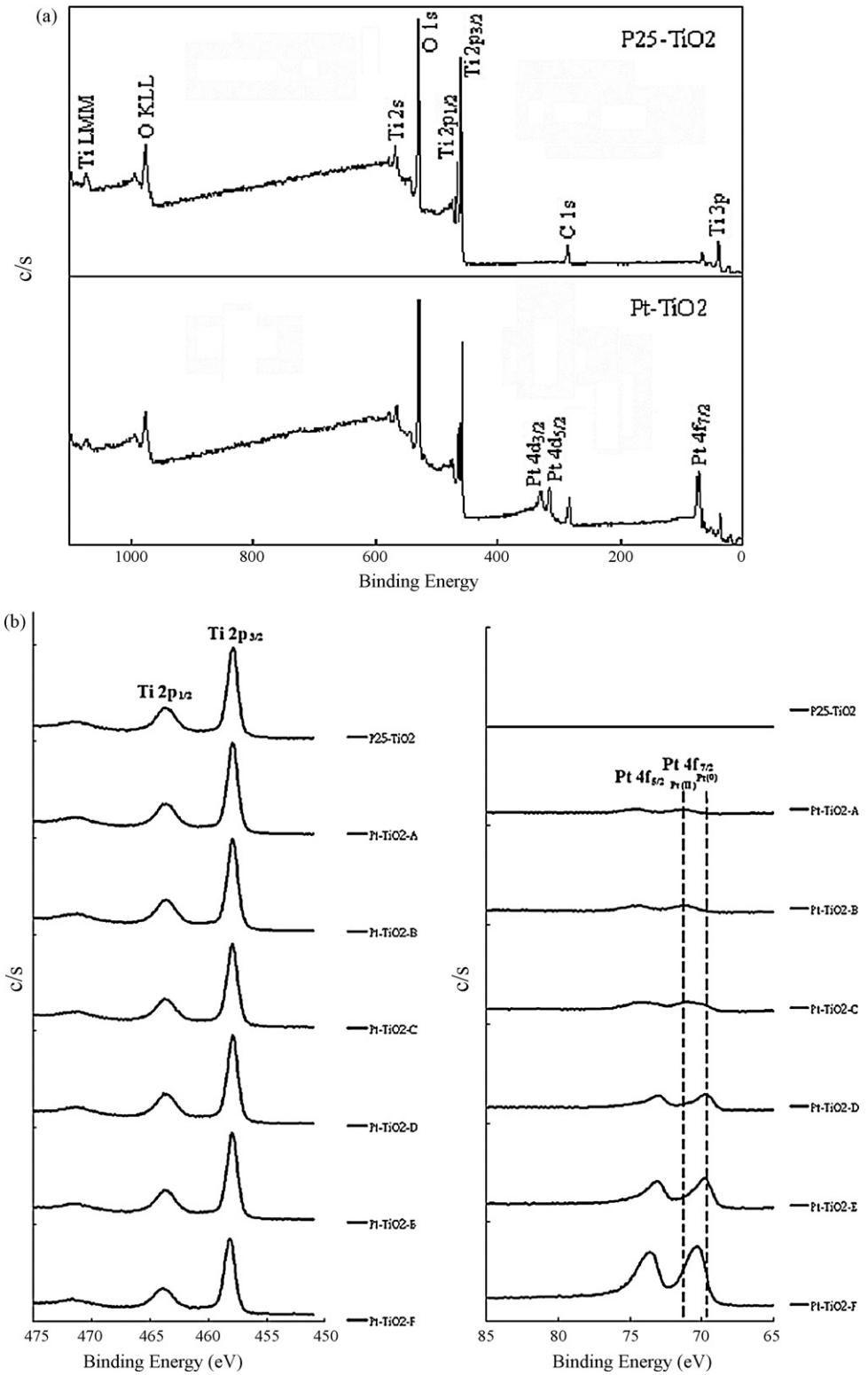

Fig. 2. XPS spectra of platinized TiO_2 after photodeposition. (a) Total survey of P25-TiO_2 and Pt-TiO_2; (b) Ti_{2p} and (c) Pt_{4f} spectra.

once the Pt concentration reaches 5.8%, Pt-TiO_2-F would act as a cut line for the competition between electron separation and recombination. With the increase of adsorption constant by introducing Pt particles, the photocatalytic reaction on platinum surface precedes a dark oxidation reaction on Pt or other metal surface [26,28]. However, more Pt dopant, such as Pt-TiO_2-G, did only mediate less photocatalytic activity comparing with Pt-TiO_2-F (Fig. 3). In the Pt-TiO_2-mediated photodegradation of trichloroethylene, similar phenomena were observed [29].

That a major role of surface deposition of rather smaller Pt clusters on TiO_2 is attributed could be explained as following. First, to accelerate the formation of $O_2^{\bullet-}$ with the increase of charge separation, thus the recombination decreases and product yields increase, initiated by h^+ or $^{\bullet}OH$ as shown in Fig. 4. The varied roles

Table 1
Physical properties of the platinum deposits TiO_2 ratios (wt%).

Catalyst	Pt/TiO_2 (wt%)[a]	Specific surface area (m^2/g)	Pore volume (cm^2/g)	XPS element atomic ratio (%)		EDS element atomic ratio (%)		
				Pt	Ti	Pt	Ti	O
P25-TiO_2	0	55.4202	0.017926	0	100	0	30.06	69.94
Pt-TiO_2-A	0.4	51.7638	0.015025	0.7	99.3	0.08	27.18	72.14
Pt-TiO_2-B	0.8	51.9193	0.015098	1.5	98.5	0.14	26.64	73.22
Pt-TiO_2-C	1.6	48.9934	0.014187	2.6	97.4	0.23	25.91	73.86
Pt-TiO_2-D	4	53.6359	0.015490	3.3	96.7	0.39	25.40	74.21
Pt-TiO_2-E	8	52.4498	0.015229	4.6	95.4	0.68	24.63	74.69
Pt-TiO_2-F	16	51.2637	0.014968	5.8	94.2	0.92	24.01	75.07
Pt-TiO_2-G	40	53.7354	0.016673	7.1	92.9	1.73	23.37	74.90

[a] Weight percentage of Pt for Pt-TiO_2 prepared by a photochemical impregnation method.

assigned to platinum clusters, Pt_n as a function of size, are shown in Eqs. (1)–(3). In addition, in photocatalytic reactions in the presence of molecular oxygen, the doping metal reduces O_2 by conducting band electrons, and then promotes the rate-limiting step (Eq. (2)) [30].

$$Pt_n + e^- \rightarrow Pt_n{}^- \quad (1)$$

$$Pt_n{}^- + O_2 \rightarrow O_2{}^{\bullet -} + Pt_n \quad (2)$$

$$Pt_n{}^- + h^+ \rightarrow Pt_n \quad (3)$$

It could be assumed that, upon depositing noble metal nanoparticles on the surface of the TiO_2, the quantum yields of the photodestruction reaction increase. Both $O_2{}^{\bullet -}$ and $^{\bullet}OH$ radicals facilitated oxygen reduction, which could be the rate determining step of the oxidation reactions as shown in Fig. 4.

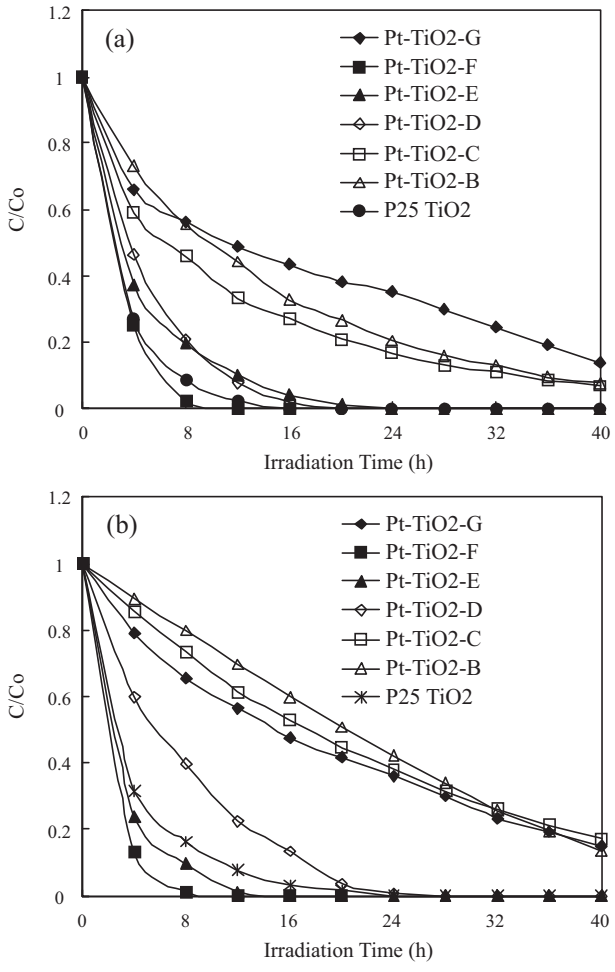

Fig. 3. Temporal course of the photodegradation of CV (0.05 gL^{-1}, V = 100 mL) at (a) pH 9 and (b) pH 3 in aqueous suspensions containing 0.05 g platinized TiO_2 under UV irradiation.

Table 2
Comparison of maximum C/Co ratio of *N*-de-methylation between P25-TiO_2 and Pt-TiO_2 (pH 3).

pH 3				
Compounds	P25-TiO_2		Pt-TiO_2	
	Time (h)	Maximum ratio of C/Co	Time (h)	Maximum ratio of C/Co
1	0	1	0	1
2	8	0.1743	4	0.6246
3	12	0.0637	4	0.3741
4	12	0.0173	4	0.1473
5	12	0.0110	4	0.0413
6	16	0.0945	4	0.1299
7	16	0.0018	4	0.0425
8	20	0.0010	4	0.0205
9	24	0.0005	8	0.0058
10	28	0.0002	12	0.0014

3.3. Effect of pH on CV photodegradation

3.3.1. Acidic condition-(pH 3)

From the data shown in Tables 2 and 3, the Pt-TiO_2 mediated photodegradation has been monitored for more than 28 h. Products and intermediates distribution demonstrate that the maximum ratio of C/Co of the *N*-de-methylation and conjugate chromophore cleavage was formed within 4 h. Under UV irradiation for 8 h as shown in Fig. 3, the CV was degraded up to 98.9%, while the P25-TiO_2 only reached 83.5%.

The Pt-TiO_2 mediated degradation rate, in the acidic condition, depends on both adsorption rates of the reagents and the

Table 3
Comparison of maximum C/Co ratio of cleavage of conjugated chromophore structure between P25-TiO_2 and Pt-TiO_2 (pH 3).

pH 3				
Compounds	P25-TiO_2		Pt-TiO_2	
	Time (h)	Maximum ratio of C/Co	Time (h)	Maximum ratio of C/Co
11	4	0.0054	4	0.0044
12	12	0.0144	4	0.0080
13	16	0.0082	4	0.0054
14	20	0.0068	4	0.0046
15	28	0.0050	4	0.0072
16	28	0.0014	4	0.0053
23	4	0.0023	4	0.0019
24	8	0.0052	4	0.0053
25	12	0.0023	4	0.0100

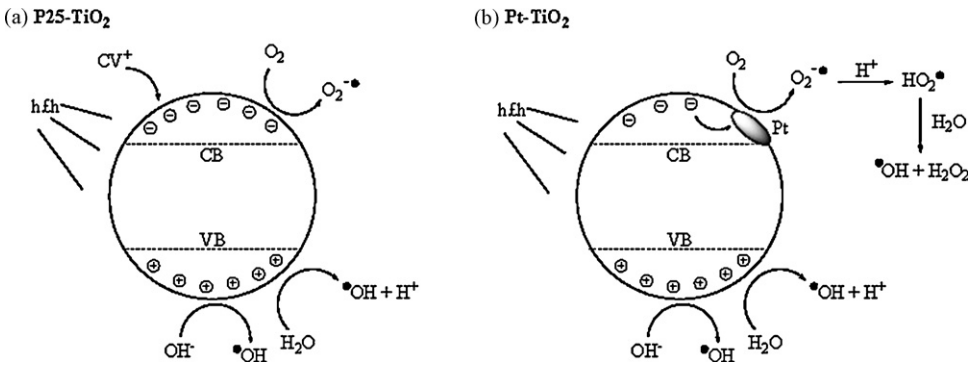

Fig. 4. Schematic representation of electron capture by (a) TiO_2 or (b) Pt-TiO_2 in contact with a semiconductor surface.

intermediates and products of photooxidation on the TiO_2 surface. The better photocatalytic ability of Pt-TiO_2 than P25-TiO_2 would be evaluated as following. Fig. 4b demonstrates that Pt-TiO_2 promotes the formation of superoxide radical anion $O_2^{\bullet -}$ (Eq. (2)) first, and under acidic condition, •OH radical is produced subsequently, as also shown in Eqs. (4)–(7). Dunn et al. reported that Pt-TiO_2 accumulated less negative species on catalyst surfaces, which deteriorated reaction rates, than pure TiO_2 in an acidic environment [31].

$$O_2^{\bullet -} + 2H^+ + e^- \rightarrow H_2O_2 \quad (4)$$

$$H_2O_2 + e^- \rightarrow {}^{\bullet}OH + OH^{\bullet -} \quad (5)$$

$$O_2^{\bullet -} + H^+ \rightarrow HO_2^{\bullet} \quad (6)$$

$$HO_2^{\bullet} + H_2O \rightarrow H_2O_2 + {}^{\bullet}OH \quad (7)$$

3.3.2. Alkaline condition—(pH 9)

Degradation products and intermediates have shown that Pt-TiO_2 mediated photodegradation activity in acidic medium is much better than in basic medium (Tables 4 and 5) for the reason that, at pH 9, the formation of active •OH species is favored. Table 4 demonstrates the maximum ratio of C/Co of the *N*-demethylation comparison in between P25-TiO_2 and Pt-TiO_2 system. The results indicate that either P25-TiO_2 or Pt-TiO_2 surface is negatively charged, thus the CV molecules are adsorbed onto the TiO_2 surface through positive ammonium groups. Again, a small amount of Pt clusters doped on TiO_2 surface accelerate the formation of $O_2^{\bullet -}$ and increase product yields initiated by h^+ or •OH as shown in the Eqs. (8) and (9).

$$h^+ + H_2O \rightarrow {}^{\bullet}OH + H^+ \quad (8)$$

$$h^+ + OH^- \rightarrow {}^{\bullet}OH \quad (9)$$

Therefore, Pt-TiO_2 photocatalytic activity in acidic medium is more than in basic medium because the surface deposition of small Pt clusters on TiO_2 is attributed to accelerate the formation of $O_2^{\bullet -}$ and •OH. Although the CV dye can, to some extent, be adsorbed onto the P25-TiO_2 or Pt-TiO_2 surface with alkaline media, when the pH value reaches 11, the CV dye molecules eventually change to a leuco compound.

3.4. Separation and identification of the intermediates

The CV degradation rate has been measured depending on initial concentration to understand the reason why platinized catalyst increases photocatalytic activity. Temporal variations of CV dye photodegradation process with UV irradiation have been characterized with HPLC-PDA–ESI-MS. The relevant change in the chromatograms recorded at 580, 350, and 300 nm is illustrated in Fig. 5. With irradiation up to 24 h, 25 components are identified with the retention time less than 50 min. The CV dye and its relevant intermediates are denoted as species **1-10**, **11-16**, and **23-25** (Table 6). Except for the initial CV dye (peak **1**), the intensities of the other peaks increased at first and subsequently decreased, indicating the formation and transformation of the intermediates.

The absorption spectra of each intermediate in the UV/visible spectral region are identified as the peaks **1-10**, **11-16**, and **23-25** in Supplementary material, Fig. 2S, respectively. The most important situation is that the hypsochromic shift of the absorption band is presumed to result from the formation of a series of *N*-de-methylated intermediates. As shown above, similar phenomena have been demonstrated once using TiO_2 in the photodegradation of Methyl Green [23] and Acid Blue 1 [24]. Above intermediates were identified as the same with the degradation of CV with TiO_2. From Table 6, the **12–16** intermediates were also

Table 4
Comparison of maximum C/Co ratio of *N*-de-methylation between P25-TiO_2 and Pt-TiO_2 (pH 9).

pH 9				
Compounds	P25-TiO_2		Pt-TiO_2	
	Time (h)	Maximum ratio of C/Co	Time (h)	Maximum ratio of C/Co
1	0	1	0	1
2	8	0.2740	4	0.3231
3	12	0.1323	8	0.1336
4	12	0.0340	12	0.0362
5	16	0.0210	16	0.0238
6	16	0.0334	16	0.0360
7	20	0.0018	20	0.0187
8	24	0.0035	24	0.0042
9	24	0.0038	24	0.0049
10	28	0.0002	28	0.0004

Table 5
Comparison of maximum C/Co ratio of cleavage of conjugated chromophore structure between P25-TiO_2 and Pt-TiO_2 (pH 9).

pH 9				
Compounds	P25-TiO_2		Pt-TiO_2	
	Time (h)	Maximum ratio of C/Co	Time (h)	Maximum ratio of C/Co
11	4	0.0039	4	0.0012
12	8	0.0127	8	0.0016
13	8	0.0092	12	0.0006
14	8	0.0046	12	0.0001
15	12	0.0068	16	0.0007
16	20	0.0019	24	0.0004
23	8	0.0007	8	0.0006
24	12	0.0049	16	0.0014
25	20	0.0029	28	0.0019

Table 6
The photo-decomposed intermediates of CV by Pt-TiO_2/UV process.

HPLC peaks	Intermediates	ESI-MS spectrum ions (*m*/*z*)	Absorption maximum (nm)
1	*N*,*N*,*N*′,*N*′,*N*″,*N*″,-hexamethyl pararosaniline	372.51	588.3
2	*N*,*N*-dimethyl-*N*′,*N*′-dimethyl-*N*″,-methyl pararosaniline	358.56	581.0
3	*N*,*N*-dimethyl-*N*′-methyl-*N*″,-methyl pararosaniline	344.41	573.7
4	*N*,*N*-dimethyl-*N*′,*N*′-dimethyl pararosaniline	344.35	579.8
5	*N*-methyl-*N*′-methyl-*N*″,-methyl pararosaniline	330.16	566.3
6	*N*,*N*-dimethyl-*N*′-methylpararosaniline	330.10	570.0
7	*N*-methyl-*N*′-methylpararosaniline	316.11	561.5
8	*N*,*N*-dimethylpararosaniline	316.11	566.3
9	*N*-methylpararosaniline	302.13	554.1
10	Pararosaniline	288.07	543.2
11	4-(*N*,*N*-dimethylamino)-4′-(*N*′,*N*′-dimethylamino)benzophenone	269.10	376.4
12	4-(*N*,*N*-dimethylamino)-4′-(*N*′-methylamino)benzophenone	255.07	366.6
13	4-(*N*-methylamino)-4′-(*N*′-methylamino)benzophenone	241.08	364.1
14	4-(*N*,*N*-dimethylamino)-4′-aminobenzophenone	241.05	358.8
15	4-(*N*-methylamino)-4′-aminobenzophenone	227.02	357.2
16	4,4′-Bis-aminobenzophenone	212.99	337.3
17	4-(*N*,*N*-dimethylamino)benzoic acid	N/A	365.0
18	4-(*N*-methylamino)benzoic acid	N/A	365.0
19	4-aminobenzoic acid	N/A	353.8
20	4-(*N*,*N*-dimethylamino)benzene	N/A	339.0
21	4-(*N*-methylamino)benzene	N/A	335.3
22	4-aminobenzene	N/A	311.5
23	4-(*N*,*N*-dimethylamino)phenol	138.22	309.7
24	4-(*N*-methylamino)phenol	124.25	283.5
25	4-aminophenol	110.03	278.1

identified as the same with the degradation of **11** with Pt-TiO_2 (Table 1S).

The photo-decomposed intermediates were further identified with HPLC–ESI mass spectrometric method as shown in Table 6. The molecular ion peaks appeared to be in the acid forms of the intermediates (Supplementary material, Fig. 3S). From the results of mass spectral analysis, the component **1**, *m*/*z* = 372.51, was confirmed. The other components were **2**, *m*/*z* = 358.56; **3**, *m*/*z* = 344.41; **4**, *m*/*z* = 344.35; **5**, *m*/*z* = 330.10; **6**, *m*/*z* = 330.16; **7**, *m*/*z* = 316.11; **8**, *m*/*z* = 316.11; **9**, *m*/*z* = 302.13; **10**, *m*/*z* = 288.07; **11**, *m*/*z* = 269.24; **12**, *m*/*z* = 255.01; **13**; **14**, *m*/*z* = 271.05; **15**, *m*/*z* = 227.02; **16**, *m*/*z* = 212.99; **23**, *m*/*z* = 138.22; **24**, *m*/*z* = 124.05 and **25**, *m*/*z* = 110.00. Moreover, the relative distribution and time reaching maximum concentration of the *N*-de-methylated and oxidative cleavage reaction of conjugated chromophore structure intermediates obtained are illustrated. In accordance with data shown in Fig. 6, the successive appearance of the maximum distribution of each intermediate, such as **2**–**10**, **11**–**16**, and **23**–**25**, indicates that the stepwise process of CV *N*-de-methylation has occurred.

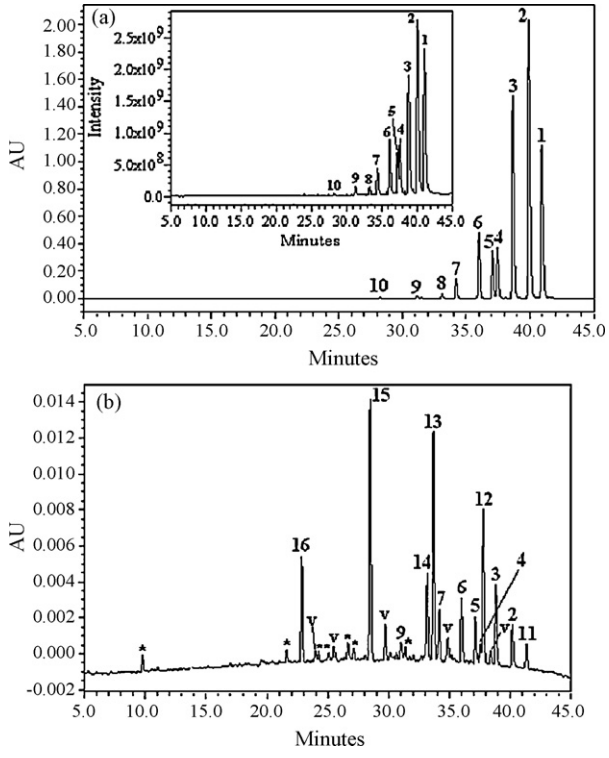

Fig. 5. HPLC chromatogram of the intermediates with Pt-TiO_2-F 0.5 gL^{-1}, pH 9. (a) Total ion chromatogram, recorded at 580 nm, (b) 350 nm and (c) 300 nm, at 24 h of irradiation.

3.5. Proposed mechanism of CV degradation

Under the UV irradiation, most of the •OH radicals are generated directly from the reaction between the holes and surface-adsorbed H_2O or OH^-. However, the probability for the formation of $O_2^{\bullet-}$ should be much less than that of •OH [32]. With regard to Pt-TiO_2-mediated photacatalysis process under acidic condition, the pathway to form $O_2^{\bullet-}$ should be much favored than that of •OH radical. The *N*-de-methylation of the CV dyes occurs mostly by the attack of the $O_2^{\bullet-}$ and •OH species on the *N*, *N*-dimethyl groups of the CV dye. Once adding Pt particles onto TiO_2, the photodegradation intermediates distribution is changed. There is no significant conjugated chromophore structure cleavage being identified from the experiments as discussed above.

On the other hand, under alkaline conditions, especially in the Pt-TiO_2-F system, the first product (**2**) of *N*-de-methylation reached its maximum concentrations after a 4 h irradiation period (Fig. 6b, curve **2**). Further degradation of formation intermediates, such as **3-4**, **5-6**, and **7-8**, reached the maximum concentrations after the irradiation period of 8–12, 16, and 16–20 h, respectively (Fig. 6a, curves **3-4**, **5-6**, and **7-8**). In the case of P25-TiO_2 system, the intermediates as **2**, **3-4**, **5-6**, and **7-8**, reached its maximum concentrations after irradiation for 8, 12, 16–20, and 20–24 h, respectively (Fig. 6a, curves **2**, **3-4**, **5-6**, and **7-8**). The •OH radicals attacked the mono-, di-, tri-, and tetra-methyl groups resulting in **2**, **3-4**, **5-6**, and **7-8** compounds, which could be mainly produced during the *N*-de-methylation steps. Moreover, both **11** and **23** are stepwise *N*-de-methylated to yield compounds **16** and **25**. It should be emphasized here that upon the mechanisms, all aforementioned

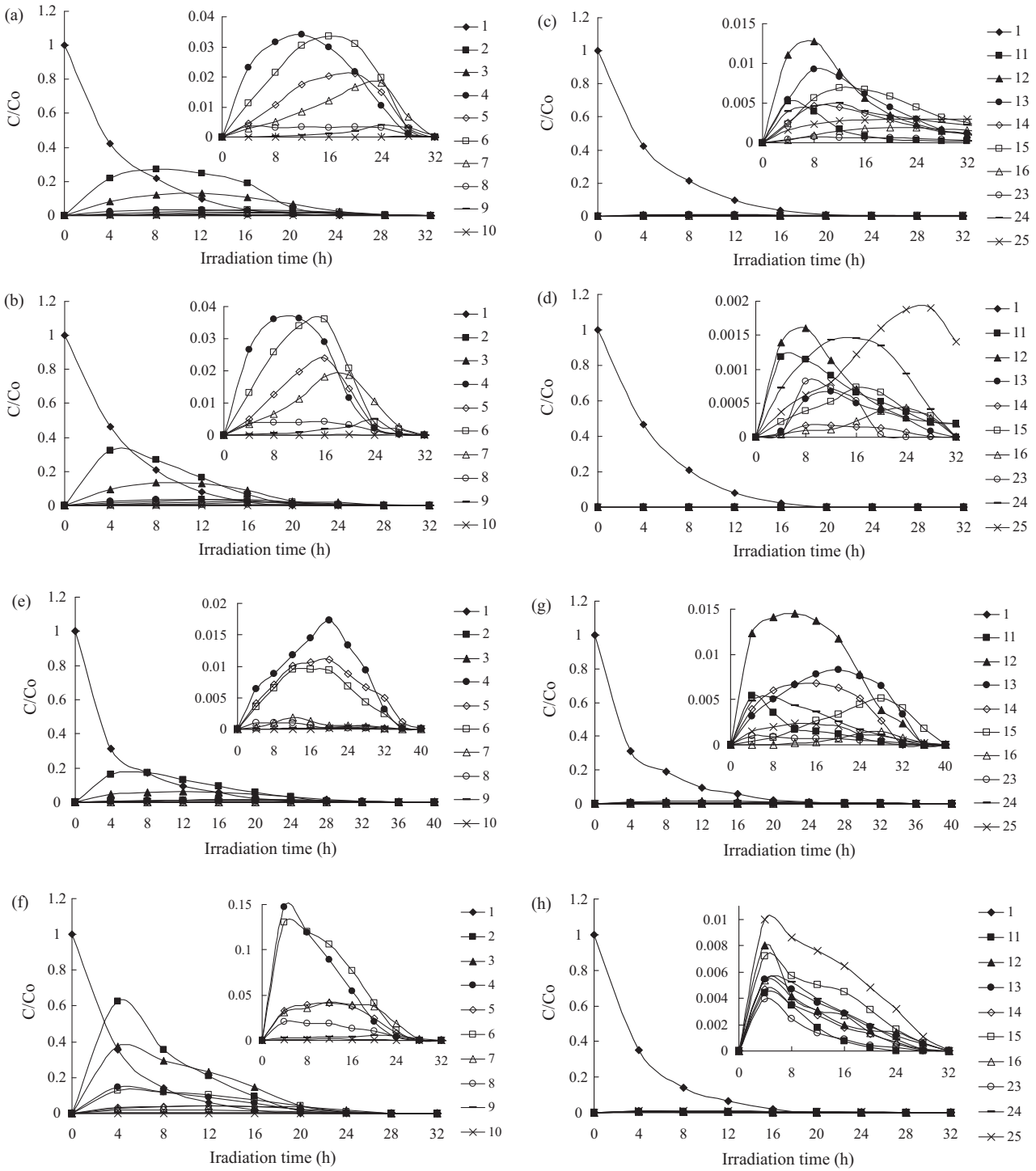

Fig. 6. Variation in the relative distribution of the *N*-de-methylated and cleavage of conjugated chromophore structure products obtained from the photodegradation of the CV dye as a function of the irradiation time. Curves **1**-**10**, **11**-**16**, and **23**-**25** correspond to the peaks **1**-**10**, **11**-**16**, and **23**-**25**, in Fig. 5, respectively. Conditions: (a) P25-TiO_2, pH 9, **1-10** intermediates; (b) Pt-TiO_2, pH 9, **1-10** intermediates; (c) P25-TiO_2, pH 9, **11-16** and **23-25** intermediates; (d) Pt-TiO_2, pH 9, **11-16** and **23-25** intermediates; (e) P25-TiO_2, pH 3, **1-10** intermediates; (f) Pt-TiO_2, pH 3, **1-10** intermediates; (g) P25-TiO_2, pH 3, **11-16** and **23-25** intermediates; (h) Pt-TiO_2, pH 3, **11-16** and **23-25** intermediates.

processes rely on O_2 to promote the cleavage of the CV conjugated chromophore structure.

However, from the two different results as shown above, the pH effect did show that the formation rate of intermediates increases as the $^{\bullet}OH$ or $O_2^{\bullet-}$ concentration increases, until a critical $^{\bullet}OH$ or $O_2^{\bullet-}$ concentration is achieved. Although, photocatalytic activity strongly depends on the amount of Pt modified onto a TiO_2 surface, the mechanistic analysis does demonstrate that degradation pathway has led most oxidative *N*-de-alkylation processes being preceded by the formation of nitrogen-centered radical, whereas the destruction of the dye chromophore structures proceeded by the generation of the carbon-centered radical [23,24]. It is well known that the potential of multi-electron reduction of O_2 (e.g. $O_2 + 2H^+ + 2e^- = H_2O_{2(aq)}$, +0.682 V; $O_2 + 4H^+ + 4e^- = 2H_2O$, +1.23 V) is more positive than for the single-electron process (e.g. $O_2 + e^- = O_2^{\bullet-}{}_{(aq)}$, −0.284 V; $O_2 + H^+ + e^- = HO_2^{\bullet}$, −0.046 V vs. NHE). It seems reasonable to consider that such multi-electron reductions more readily precede on the surface of Pt that works as an

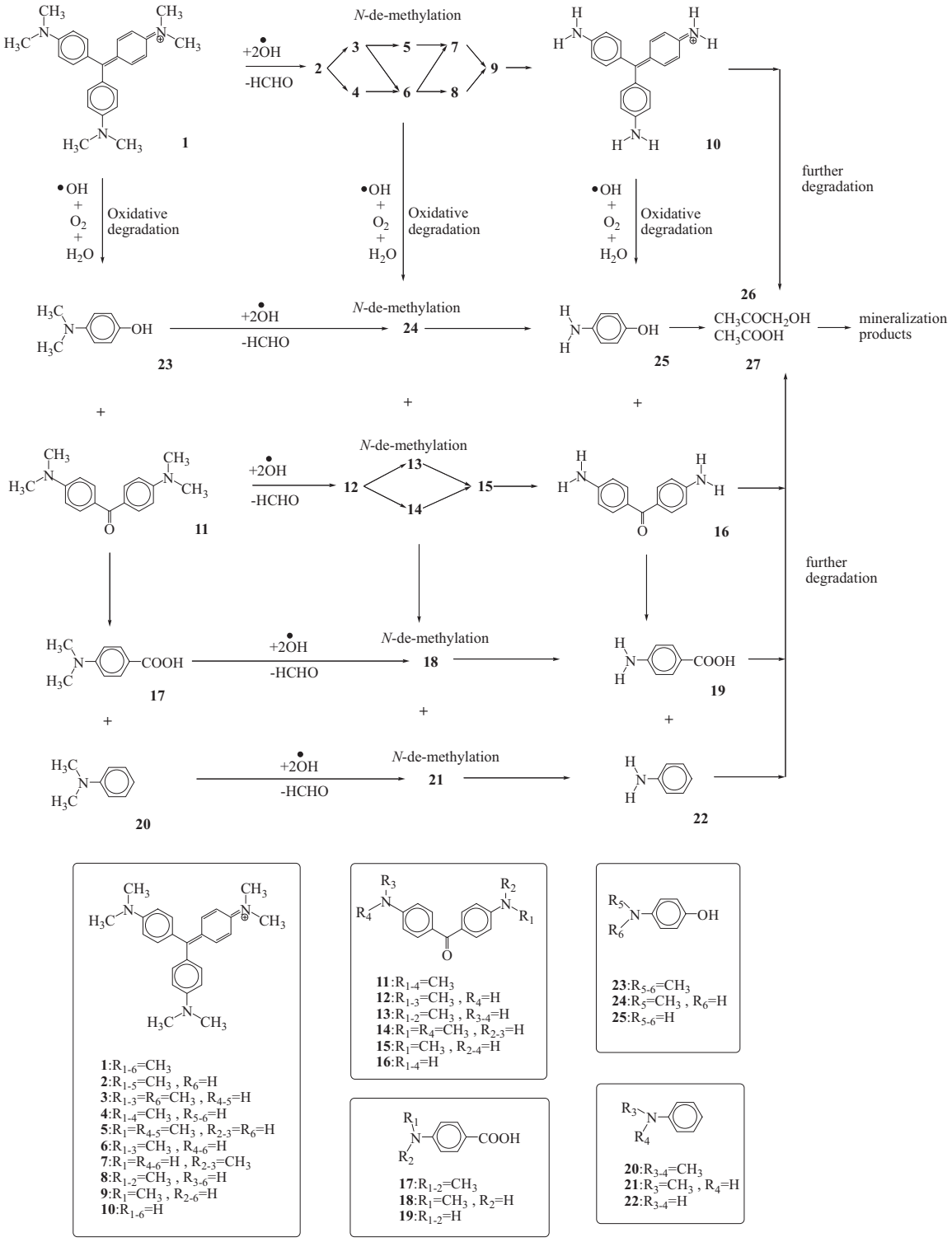

Fig. 7. Proposed photodegradation mechanism of the CV dye under UV irradiation in aqueous Pt-TiO_2 dispersions followed by the identification of several intermediates by HPLC–ESI mass spectral techniques.

electron pool and catalyzes O_2 reduction, comparing to the bare surface of oxide semiconductors [33–35]. The high CV photodegradation activity mediated by Pt-TiO_2 is due to the promotion of multi-electron reduction of O_2 on the Pt co-catalyst rather than single-electron reduction [36,37].

Based on the above experimental results, the degradation pathway is tentatively proposed as depicted in Fig. 7. Firstly, the cationic CV dye molecule was adsorbed on Pt-TiO_2 surface through charge attraction. Under UV irradiation, the conduction band electrons flow from the valence band to the metal (i.e. to a Pt site), and the Schottky barrier acts as an efficient electron trap to decrease the recombination rate. The hydrolysis or deprotonation reaction of CV dye yielded a nitrogen-centered radical. Once attacked by •OH radicals, *N*-de-methylation occurred as shown in Fig. 7. The mono-de-methylated dye, **2**, could also be adsorbed on Pt/TiO_2 particle surface and involved in the similar mechanistic process.

However, the •OH radicals could attack the conjugated structure and produce a carbon-centered radical. Moreover, m dye derivatives, **11** and **23**, are formed eventually. Moreover, the species **11** and **23** can also be implicated in *N*-de-methylation to yield **12** and **24**, respectively. The *N*-de-methylation processes continue to really form *N*-de-methylated dye, **10**, **16** and **25**. Further oxidation can lead the ring-opening and the formation of aliphatic oxidation products (compounds **17-19** and **20-22**).

4. Conclusion

The modified TiO_2 with metal nanoparticles (Pt), compared with pure TiO_2, has enhanced the photocatalytic degradation of CV. The results indicated that Pt-TiO_2-F (5.8 wt% Pt loading) gave the highest photocatalytic activity. Both *N*-de-methylation and the destruction of the conjugated structure of the CV dye took place on the TiO_2 and Pt-TiO_2. The platinization of TiO_2 not only enhanced the degradation rate but also demonstrated different degradation pathway. In the pure TiO_2-mediated photocatalysis, *N*-de-methylation preferred being under alkaline condition, and the destruction of the conjugated structure preferred being under acidic condition. Interestingly, in the Pt-TiO_2-mediated photocatalysis process, it demonstrates a total reverse result. *N*-de-methylation reaction took place under acidic condition, while the destruction of the conjugated structure preferred under alkaline condition. Pt-TiO_2 enhanced electron transfer in an acidic condition, resulting the competition of $O_2^{\bullet-}$ with •OH radicals in the *N*-de-methylation degradation of CV. This is the first report demonstrating the mechanistic differences of the Pt-TiO_2 photocatalyst towards the photodegradation of triphenylmethane dye. Most of the intermediates and final products have been identified by HPLC–ESI-MS and UV–visible spectra.

Acknowledgment

This research was supported by the National Science Council of the Republic of China (NSC 97-2113-M-438-002-MY2; NCS 98 2622-M-142-001-CC1).

Appendix A. Supplementary data

Supplementary data associated with this article can be found, in the online version, at doi:10.1016/j.jhazmat.2010.09.022.

References

[1] Ullmann's Encyclopedia of Industrial Chemistry. Part A27. Triarylmethane and Diarylmethane Dyes. 6th Ed., Wiley-VCH, New York, 2001.
[2] M.S. Baptista, G.L. Indig, Effect of BSA binding on photophysical and photochemical properties of triarylmethane dyes, J. Phys. Chem. B 102 (1998) 4678–4688.
[3] A.C. Bhasikuttan, A.V. Sapre, L.V. Shastri, Photoinduced electron transfer in crystal violet (CV^+)-bovine serum albumin (BSA) system: evaluation of reaction paths and radical intermediates, J. Photochem. Photobiol. A: Chem. 150 (2002) 59–66.
[4] L.M. Lewis, G.L. Indig, Effect of dye aggregation on triarylmethane-mediated photoinduced damage of hexokinase and DNA, J. Photochem. Photobiol. B: Biol. 67 (2002) 139–148.
[5] R. Bonnett, G. Martinez, Photobleaching of sensitisers used in photodynamic therapy, Tetrahedron 57 (2001) 9513–9547.
[6] B.P. Cho, T. Yang, L.R. Blankenship, J.D. Moody, M. Churchwell, F.A. Bebland, S.J. Culp, Synthesis and characterization of *N*-demethylated metabolites of Malachite Green and Leucomalachite Green, Chem. Res. Toxicol. 16 (2003) 285–294.
[7] T.L. Thompson, J.T. Yates, Surface science studies of the photoactivation of TiO_2—new photochemical processes, Chem. Rev. 106 (2006) 4428–4453.
[8] O. Carp, C.L. Huisman, A. Reller, Photoinduced reactivity of titanium dioxide, Prog. Solid State Chem. 32 (2004) 33–177.
[9] J. Tang, J.R. Durrant, D.R. Klug, Mechanism of photocatalytic water splitting in TiO_2. Reaction of water with photoholes, importance of charge carrier dynamics, and evidence for four-hole chemistry, J. Am. Chem. Soc. 130 (2008) 13885–13891.
[10] R.A. May, M.N. Patel, K.P. Johnston, K.J. Stevenson, Flow-based multiadsorbate ellipsometric porosimetry for the characterization of mesoporous Pt-TiO_2 and Au-TiO_2 nanocomposites, Langmuir 25 (2009) 4498–4509.
[11] P. Du, J. Schneider, F. Li, W. Zhao, U. Patel, F.N. Castellano, R. Eisenberg, Bi-terpyridyl platinum(II) chloro complexes: molecular catalysts for the photogeneration of hydrogen from water or simply precursors for colloidal platinum, J. Am. Chem. Soc. 130 (2008) 5056–5058.
[12] M. Ren, R. Ravikrishna, K.T. Valsaraj, Photocatalytic degradation of gaseous organic species on photonic band-gap titania, Environ. Sci. Technol. 40 (2006) 7029–7033.
[13] J. Hensel, G. Wang, Y. Li, J.Z. Zhang, Synergistic effect of CdSe quantum dot sensitization and nitrogen doping of TiO_2 nanostructures for photoelectrochemical solar hydrogen generation, Nano Lett. 10 (2010) 478–483.
[14] X. Fu, W.A. Zeltner, M.A. Anderson, The gas-phase photocatalytic mineralization of benzene on porous titania-based catalysts, Appl. Catal. B: Environ. 6 (1995) 209–224.
[15] J.L. Falconer, K.A. Magrini-Bair, Photocatalytic and thermal catalytic oxidation of acetaldehyde on Pt/TiO_2, J. Catal. 179 (1998) 171–178.
[16] Y. Nosaka, K. Koenuma, K. Ushida, A. Kira, Reaction mechanism of the decomposition of acetic acid on illuminated TiO_2 powder studied by means of *in Situ* electron spin resonance measurements, Langmuir 12 (1996) 736–738.
[17] Z. Jin, Z. Chen, Q. Li, C. Xi, X. Zheng, On the conditions and mechanism of PtO_2 formation in the photoinduced conversion of H_2PtCl_6, J. Photochem. Photobiol. A: Chem. 81 (1994) 177–182.
[18] A.V. Vorontsov, E.N. Savinov, Z. Jin, Influence of the form of photodeposited platinum on titania upon its photocatalytic activity in CO and acetone oxidation, J. Photochem. Photobiol. A: Chem. 125 (1999) 113–117.
[19] Y. Ishibai, J. Sato, S. Akita, T. Nishikawa, S. Miyagishi, Photocatalytic oxidation of NO_x by Pt-modified TiO_2 under visible light irradiation, J. Photochem. Photobiol. A: Chem. 188 (2007) 106–111.
[20] W. Zhao, C. Chen, X. Li, J. Zhao, H. Hidaka, N. Serpone, Photodegradation of sulforhodamine-B dye in platinized titania dispersions under visible light irradiation: influence of platinum as a functional Co-catalyst, J. Phys. Chem. B 106 (2002) 5022–5028.
[21] H. Park, W. Choi, Photocatalytic reactivities of nafion-coated TiO_2 for the degradation of charged organic compounds under UV or visible light, J. Phys. Chem. B 109 (2005) 11667–11674.
[22] X. Hu, T. Mohamood, W. Ma, C. Chen, J. Zhao, Oxidative decomposition of Rhodamine B dye in the presence of VO_2^+ and/or Pt(IV) under visible light irradiation: *N*-deethylation, chromophore oxidative cleavage reaction, and mineralization, J. Phys. Chem. B 110 (2006) 26012–26018.
[23] C.C. Chen, C.S. Lu, Mechanistic studies of the photocatalytic degradation of Methyl Green: an investigation of products of the decomposition processes, Environ. Sci. Technol. 41 (2007) 4389–4396.
[24] C.C. Chen, H.J. Fan, J.L. Jan, Degradation pathways and efficiencies of Acid Blue 1 by photocatalytic reaction with ZnO nanopowder, J. Phys. Chem. C 112 (2008) 11962–11972.
[25] U. Siemon, D. Bahnemann, J.J. Testa, D. Rodriguez, M.I. Litter, N. Bruno, Heterogeneous photocatalytic reactions comparing TiO_2 and Pt/TiO_2, J. Photochem. Photobiol. A: Chem. 148 (2002) 247–255.
[26] A.V. Vorontsov, I.V. Stoyanova, D.V. Kozlov, V.I. Simagina, E.N. Savinov, Kinetics of the photocatalytic oxidation of gaseous acetone over platinized titanium dioxide, J. Catal. 189 (2000) 360–369.
[27] A.V. Vorontsov, E.N. Savinov, Z. Jin, Influence of the form of photodeposited platinum on titania upon its photocatalytic activity in CO and acetone oxidation, J Photochem Photobiol A: Chem. 125 (1999) 113–117.
[28] F.B. Li, X.Z. Li, The enhancement of photodegradation efficiency using Pt-TiO_2 catalyst, Chemosphere 48 (2002) 1103–1111.
[29] M.D. Driessen, V.H. Grassian, Photooxidation of trichloroethylene on Pt/TiO_2, J. Phys. Chem. B 102 (1998) 1418–1423.
[30] R. Abe, H. Takami, N. Murakami, B. Ohtani, Pristine simple oxides as visible light driven photocatalysts: highly efficient decomposition of organic compounds over platinum-loaded tungsten oxide, J. Am. Chem. Soc. 130 (2008) 7780–7781.
[31] W.W. Dunn, Y. Aikawa, A.J. Bard, Characterization of particulate titanium dioxide photocatalysts by photoelectrophoretic and electrochemical measurements, J. Am. Chem. Soc. 100 (1981) 3456–3459.
[32] C.C. Chen, C.S. Lu, Photocatalytic degradation of Basic Violet 4: degradation efficiency, product distribution, and mechanisms, J. Phys. Chem. C 111 (2007) 13922–13932.
[33] Y.S. Ma, C.N. Chang, Y.P. Chiang, H.F. Sung, A.C. Chao, Photocatalytic degradation of lignin using Pt/TiO_2 as the catalyst, Chemosphere 71 (2008) 998–1004.
[34] N. Murakami, O.P. Prieto Mahaney, R. Abe, T. Torimoto, B. Ohtani, Double-beam photoacoustic spectroscopic studies on transient absorption of titanium(IV) oxide photocatalyst powders, J. Phys. Chem. C 111 (2007) 11927–11935.
[35] C. Kormann, D. Bahnemann, M.R. Hofmann, Photocatalytic production of hydrogen peroxides and organic peroxides in aqueous suspensions of titanium dioxide, zinc oxide, and desert sand, Environ. Sci. Technol. 22 (1988) 798–806.
[36] M. Mrowetz, W. Balcerski, A.J. Colussi, M.R. Hoffmann, Oxidative power of nitrogen-doped TiO_2 photocatalysts under visible illumination, J. Phys. Chem. B 108 (2004) 17269–17273.
[37] T. Hirakawa, Y. Nosaka, Properties of $O_2^{\bullet-}$ and OH• formed in TiO_2 aqueous suspensions by photocatalytic reaction and the influence of H_2O_2 and some ions, Langmuir 18 (2002) 3247–3254.